Journal of Advanced Ceramics
2020, **9**(3): 312–319
https://doi.org/10.1007/s40145-020-0369-6

ISSN 2226-4108
CN 10-1154/TQ

Research Article

Preliminary 3D printing of large inclined-shaped alumina ceramic parts by direct ink writing

Liangliang YANG[a], Xiaojun ZENG[b], Allah DITTA[a], Bo FENG[a], Lizhong SU[a], Yue ZHANG[a,*]

[a]*Key Laboratory of Aerospace Materials and Performance* (*Ministry of Education*), *School of Materials Science and Engineering*, *Beihang University*, *Beijing 100191*, *China*
[b]*Department of Chemistry and Biochemistry*, *University of California Santa Barbara*, *Santa Barbara*, *California 93106*, *United States*

Received: January 7, 2020; Revised: February 23, 2020; Accepted: February 23, 2020

Abstract: Three dimensional (3D) printing technology by direct ink writing (DIW) is an innovative complex shaping technology, possessing advantages of flexibility in fabrication, high efficiency, low cost, and environmental-friendliness. Herein, 3D printing of complex alumina ceramic parts via DIW using thermally induced solidification with carrageenan swelling was investigated. The rheological properties of the slurry under different thermally-induced modes were systematically studied. The solidification properties of thermally-induced pastes with varying contents of carrageenan were optimized. The experimental results showed that the optimized paste consisting of 0.4 wt% carrageenan could be rapidly solidified at about 55 ℃, which could print inclined-plane more than 60° in vertical without support, resulting in better homogeneity of the green body. A nearly pore-free structure was obtained after sintering at 1600 ℃ for 2 h.

Keywords: three dimensional (3D) printing; alumina paste; solidification property; thermally-induced; carrageenan

1 Introduction

Three dimensional (3D) printing by direct ink writing (DIW) is a new method for materials fabrication that allows designing and rapidly fabricating materials with complex 3D shapes. Net or near-net shape components can be manufactured without the need of expensive dies, tooling, or lithographic masks, due to more freedom in geometrical design and process manipulation [1–3]. The technology has significant potential applications, such as biological materials [4–7], semiconductor materials [8], electronic materials, and thermal insulating materials [9–11]. Furthermore, the ability to print intricate-shaped ceramic materials in three dimensions by DIW is crucial for several emerging processes which necessitate preparation of the paste with uniform dispersion and high solid loading [12], precise control of micro-electromechanical systems [13,14], printing of green body with an oblique angle, and rapid solidification of the paste [15].

The ability of inclined-plane printing is essential to produce intricate-shaped 3D ceramics. The practical application of 3D printing ceramics in the industry can

* Corresponding author.
E-mail: zhangy@buaa.edu.cn

only be achieved by utilizing intricate-shape printing with inclined-plane. However, the printed wet green body with a steep incline is likely to deform or collapse, especially relating to thin-wall inclined parts. In addition, extruded paste needs to have high support strength for printing thin-walled ceramic parts with large inclination. The support strength is closely related to the viscosity for water-based ceramic paste. The higher viscosity results in the stronger deformation resistance of the paste, and can accordingly produce larger printing inclination. The inclined angle (vertical, the same with all the others) of ceramic parts is relatively higher (up to 50°), and therefore support technology is generally adopted to print such large inclination angles. However, the procedure of support technology is more complicated and it is difficult to precisely control the printing process, which significantly reduces the potential application of 3D printing technology. Currently, primary 3D printing processing techniques for inclined-plane ceramic shaping generally employ laser, binder, gels, ultraviolet (UV) or visible curable resins to retain the inclined-shape while printing green parts [16,17], such as stereolithography (SLA) [18,19], selective laser sintering (SLS), gel-printing [20–22], and binder jetting. The fabrication of ceramic parts through these shaping processes was rather cost-intensive or time-consuming [23–25]. Within the framework of these fabrication techniques, employing the thermally-induced solidification process for the inclined-plane shaping of 3D printing has attracted intensively interest due to its controllable printing progress, which may be an effective incentive method. According to our previous work [26], 3D printing of ceramics by DIW using thermally-induced solidification with carrageenan was proposed for producing complex shaped parts because of its excellent solidification property and the simple printing procedure.

The purpose of this study is to investigate the feasibility of inclined-plane printing without support technology. The thermally-induced solidification with carrageenan for ceramic paste 3D printing was adopted. As a widely used engineering ceramic, alumina was selected to prepare the experimental samples. The influences of carrageenan concentration and temperature on the rheological properties of the paste were investigated. and accordingly the paste proportions applicable for 3D printing were optimized. The properties of green bodies and sintered ceramics were characterized.

2 Experimental

2. 1 Materials

The alumina powders (SAL-161SG, Showadenko Inc., Tokyo, Japan) with an average particle diameter of 0.52 μm and a specific surface area of 6.4 m^2/g were used to prepare the concentrated alumina paste in this study. The purity of α-Al_2O_3 was over 99.33%. The alumina powders were the primary experimental raw materials. The ammonium citrate (Guoyao, Beijing, China) was used as the dispersant. Carrageenan powders (BLSW Inc., Shanghai, China), added into suspensions, were used as a thermo-curing binder to increase the viscosity of the alumina paste.

2. 2 Alumina slurry preparation and temperature optimization

In order to optimize the temperature value of process by thermally-induced solidification, 0.4 wt% carrageenan powders with optimized 0.1 wt% ammonium citrate were added into deionized ice water and mixed with alumina powders at 50 vol% solid loading. Then the alumina slurries were divided into three groups to conduct the measurements. The first slurry temperature was increased from 0 to 85 ℃ with a heating rate of 5 ℃·min^{-1}. The second slurry temperature was raised from 0 to 55 ℃ with the same heating rate of 5 ℃·min^{-1}, and the slurry was then cooled from 55 to 20 ℃ with a cooling rate of 5 ℃·min^{-1}. The third slurry temperature was also raised from 0 to 55 ℃ with the same heating rate of 5 ℃·min^{-1}; however, the heat preserved at 55 ℃ for 3 min.

2. 3 Alumina paste preparation and 3D printing

The carrageenan powders and dispersant ammonium citrate were completely mixed in deionized ice water with a certain proportion using mechanical stirring, then the alumina powders were added to the premix. The paste was mixed by a high-speed blender (JF-RVITV-150, Junfengkeji Inc., Shenzhen, China) through rotation and revolution in a vacuum atmosphere for 3 min instead of ball milling. The non-separation and uniformity of mixture were realized synchronously. The content of carrageenan powders was varied from 0.2 wt% to 0.6 wt% (per powder mixture) based on an optimized 0.11 wt% ammonium citrate (per powder mixture). The solid loading was 56 vol%.

Figure 1 shows the schematic diagram of the thermally-induced 3D ceramics process for printing Al_2O_3 ceramic parts (self-developed). At the beginning of printing, 3D models were designed by Solidworks software and sliced into the printing code by Crua software. The optimized paste was placed into a 150 mL barrel and then moved into a screw propulsion chamber by proper gas pressure. The 3D moving module was used to carry out the 3D movement of the screw extrusion module, which was controlled by a computer. The paste was extruded through a 0.4 mm brass nozzle from the propulsion chamber and subsequently solidified by hot airflow and the printing platform. The temperature of hot airflow and the print platform was 55 ℃. Finally, the nozzle could continuously print ceramic parts by controlling reasonable printing parameters. In order to maintain the excellent extrusion for 3D printing, the viscosity value of the paste should be less than 100 Pa·s, while the shear rate of the screw is 20 s^{-1}. The printing parameters were adequately selected and optimized to fabricate complex components, including propulsion gas pressure, screw rotating speed, printing speed, and *Z*-axis layer height, which are provided in Table 1.

The green bodies prepared by the technique were carefully dried at 80 ℃ for 22 h. The sample was then sintered at 1600 ℃ for 2 h with a heating rate of 3 ℃·min^{-1} in the temperature range of 25–600 ℃ and 5 ℃·min^{-1} in the temperature range of 600–1600 ℃.

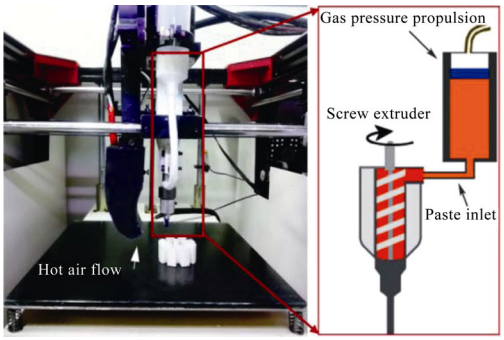

Fig. 1 Schematic diagram of the 3D process for printing alumina ceramics.

Table 1 Printing parameters for the 3D printing

Printing parameter	Value
Propulsion gas pressure	3.5 MPa
Screw rotating speed	30 r·min^{-1}
Printing speed	3 mm·s^{-1}
Z-axis layer height	0.48 mm

2.4 Characterization

The rheological properties of alumina slurries below 50 vol% solid loading were measured by a stress-controlled rheometer (R/Splus, Brookfield, USA). In thermally-induced viscosity measurements by stress-controlled rheometer, the shear rate was set at 20 s^{-1}, and the measurements were taken at temperatures ranging from 0 to 85 ℃. The scanning time was 5 s per point. Subsequently, a loss of 0.5 wt% by evaporation of water could lead to dramatic changes in viscosity when the solid loading was as high as 56 vol%. However, the testing with a stress-controlled rheometer might result in inaccurate measurements due to less moisture evaporation. Therefore, the Stokes sedimentation method was used to test the high solid loading paste [27,28]. The viscosity of the paste as high as 56 vol% solid loading could be tested in an airtight glass tube to avoid moisture loss. The parameters of Stokes sedimentation are provided in Table 2. The schematic diagram of the Stokes sedimentation method for viscosity test by thermally induction is shown in Fig. 2.

The viscosity of the solid loading paste was calculated by Eq. (1) [27].

$$\mu = \frac{d_p^2(\rho_p - \rho)g\tau}{18H} \quad (1)$$

where μ is paste viscosity, d_p, ρ_p, and ρ are the diameter of the ball, the density of the ball, and the

Table 2 Parameters of Stokes sedimentation method

Stokes sedimentation parameter	Value
Density of tungsten ball	10961.17 kg·m^{-3}
Diameter of tungsten ball	0.0089 m
Height of glass tube	0.15 m
Density of pastel	2560.01 kg·m^{-3}

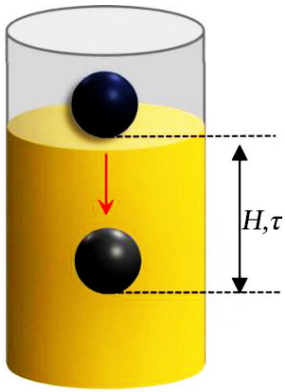

Fig. 2 Schematic diagram of the Stokes sedimentation method for viscosity test.

density of paste, respectively. H and τ are the sinking height of the ball and the sinking time of the ball. g is 9.8 N·kg^{-1}.

To ensure the accuracy of viscosity by the Stokes sedimentation method, the value of Reynolds number for the particle should be greater than 1. The Reynolds number of the particle (Re_p) was calculated by Eq. (2) [28].

$$Re_p = \frac{d_p H \rho}{\mu \tau} \quad (2)$$

The relative sintered density of sintered Al_2O_3 ceramics was measured by Archimedes′ method, and the bending strength of the samples was determined by three-point bending method. The samples, with the size of 3 mm × 4 mm × 40 mm, were prepared by grinding and polishing. The tests were carried out on an Instron-5500 machine with a span width of 32 mm and a loading rate of 0.5 mm·min^{-1}. A total of 15 samples were employed for the testing, and the average value was determined. The Vickers hardness was determined using a microhardness tester (Model: TUKONTM 2500, Wilson, New York, USA) on the polished surface of the samples with a load of 5 kg and dwell time of 15 s. A total of 10 indentations were made on the surface of each sample for micro-hardness. The homogeneity of the green body and the fracture surfaces of sintered samples were observed by scanning electron microscopy (SEM, JSM-7500, Tokyo, Japan).

3 Results and discussion

3.1 Optimization of thermally-induced temperature

Figure 3 plots the rheological properties of the slurry with different thermally-induced measurements.

It was observed in Figs. 3(a) and 3(b) that the viscosity of the ceramic slurry was almost constant in the temperature range of 0–40 ℃. However, the viscosity of paste increased rapidly with the rise of temperature from 40 to 55 ℃ in 3 min. When the temperature continued to ascend from 55 to 60 ℃, the viscosity of the paste decreased rapidly and then remained almost constant, as shown in Fig. 3(a). Thus, it might be concluded that carrageenan following complete dissolution in the paste could later almost entirely disentangle with the increase of temperature from 55 to 60 ℃ causing rapid decline in the viscosity of the slurry; however, the further slight decrease in

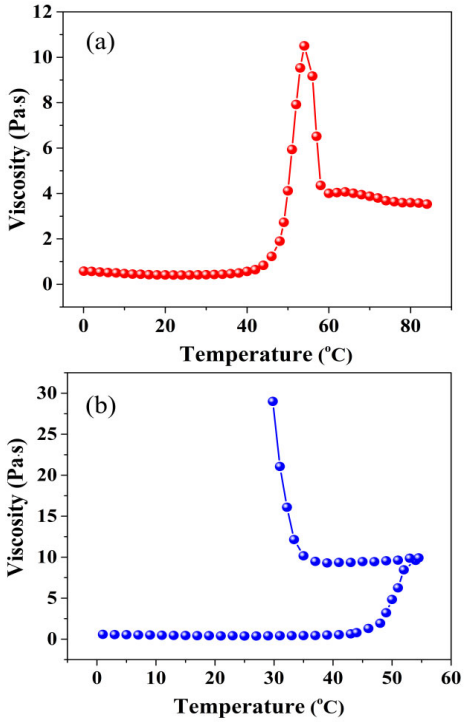

Fig. 3 Viscosity property of alumina slurry with 0.4 wt% carrageenan thermally-induced: (a) on heating and (b) on heating and then on cooling (solid loading was 50 vol%).

viscosity in the temperature range of 60–85 ℃ was ascribed to Brownian motion intensified. The slurry formed a viscous polymer solution and the viscosity value was still higher than before the carrageenan dissolution in the paste. Subsequently, it was observed in Fig. 3(b) that the viscosity of paste remained constant and increased rapidly in the case of cooling the slurry from 55 to 20 ℃. The phenomenon indicated that carrageenan mixed in the slurry starts to swell and absorb water freely. This caused the carrageenan to fully expand and absorb free water when the temperature was raised to 55 ℃. When the carrageenan was fully dissolved at 55 ℃, the viscosity of the slurry decreased with increasing temperature, depending on the properties of the dissolved carrageenan [29–33]. Simultaneously, in the cooling stage, when the slurry was cooled to nearly 30 ℃, the viscosity of the slurry increased rapidly because the carrageenan quickly solidified and formed a gel.

Figure 4 shows the variation in the viscosity of the slurry, contained 0.4 wt% carrageenan, during heating from 0 to 55 ℃ and heat preservation at 55 ℃. It was noticeable that the viscosity of the ceramic slurry kept almost constant in the heat preservation phase, which further verified that carrageenan fully dissolved at 55 ℃.

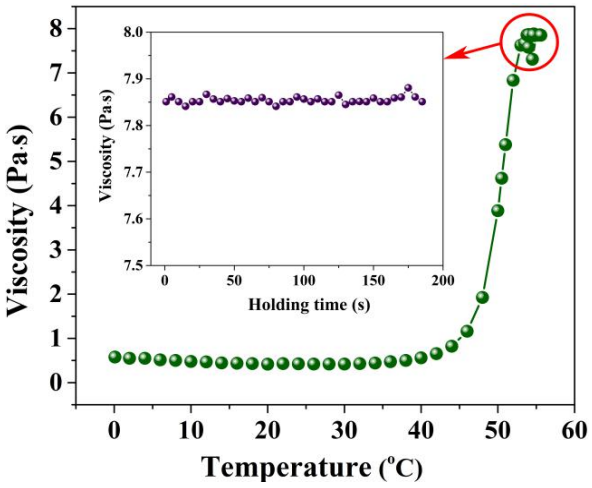

Fig. 4 Viscosity property of alumina slurry with 0.4 wt% carrageenan on heating (solid loading was 50 vol%).

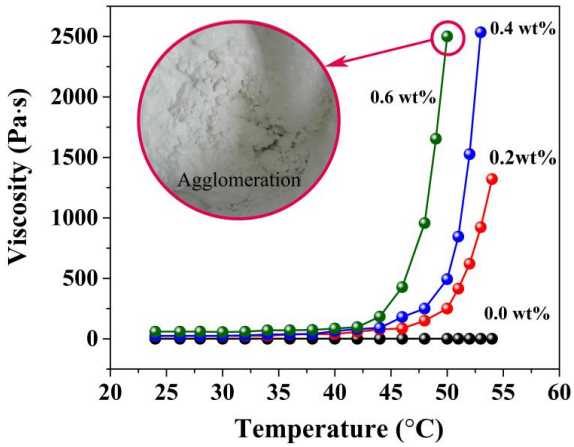

Fig. 5 Solidification properties of alumina slurries with different carrageenan concentrations on heating (solid loading of 56 vol%).

In summary, the appropriate content of carrageenan was added in ceramic slurry, and subsequently the mixture was quickly heated to 55 ℃. Most of the free water in the slurry was lost, resulting in an increase of viscosity. In the condition of high solid loading, the loss of very little free moistures could bring about rapid curing of the paste, and therefore it was feasible to achieve solidification by this mechanism. In order to achieve rapid curing during 3D printing, the carrageenan needed to swell and absorb water as the temperature increases. Thus, free water in the paste was reduced, and the solid loading of the paste was rapidly increased.

3. 2 Solidification properties of alumina paste using thermally induced method

In order to investigate the influence of carrageenan concentration on the viscosity of alumina paste with a solid loading of 56 vol%, alumina pastes with different carrageenan contents were prepared and heated from 23 to 55 ℃ in 6 min. Figure 5 shows the viscosity of different concentrations of carrageenan (based on water) under heating.

The viscosity increased slightly with the increase of the concentration of carrageenan in the range of 23–40 ℃. However, when the temperature continued to rise, the viscosity increased significantly. The viscosity of paste increased when both carrageenan concentration and temperature increased, while the viscosity of the paste without carrageenan had no effect on temperature below 55 ℃. The viscosity of the paste containing 0.4 wt% carrageenan increased sharply, while paste containing 0.2 wt% carrageenan increased less than others. The increase in viscosity was attributed to the swelling of carrageenan and the absorption of water with the rise of temperature below 55 ℃ when the paste was heated. The viscosity of the paste increased with the content of carrageenan increasing on the condition of heating above 55 ℃, and the high concentration of carrageenan could absorb more free water. Simultaneously, the viscosity of the paste with 0.6 wt% carrageenan increased more sharply than 0.4 wt% carrageenan and the agglomeration occurred in the paste and presented a discontinuous characteristic. This phenomenon indicated that carrageenan in an excessively high concentration swelled in paste and plenty of water was absorbed when the temperature was about 55 ℃. The high concentration of carrageenan would make solidifications where some paste firstly contacted at high temperature while others were at a relative lower temperature, which made the paste presented a discontinuous characteristic.

Based on several groups of experiments, 0.4 wt% carrageenan was selected as optimized thermally-induced 3D printing paste.

Figures 6(a) and 6(b) display the printed inclined-plane samples. The inclined angle of the sample was as high as 30°. It was indicated that the body had a sufficiently high strength to ensure that the printing of the inclined surface with thermally-induced solidification. Figure 6(c) shows the fracture surface morphology of interlamination for the printed green body and the sintered sample. It was observed that the extrusion of the paste between the layers had proper fusion and no obvious defects were found. The sintered sample was in accordance with the green body. This was due to the

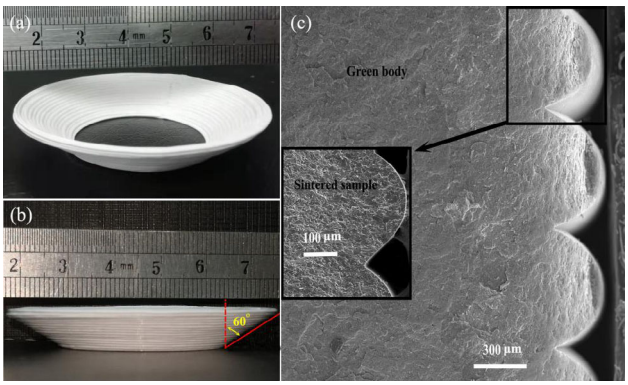

Fig. 6 Printed inclined-plane samples: (a, b) the green body with 60° inclined-plane printed and (c) the fracture surface morphology of interlamination for the printed green body and the sintered sample.

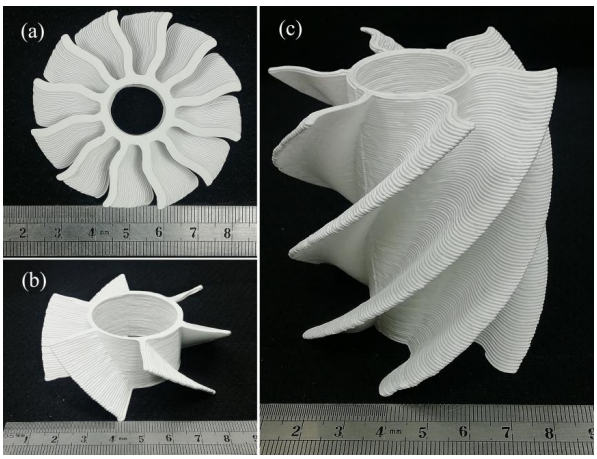

Fig. 7 Printed impeller samples of the Al_2O_3 green body.

appropriate interval time between layers and rapid solidification with optimized temperature and carrageenan content.

The printing tests revealed that 0.4 wt% carrageenan with 56 vol% solid loading was the minimum dosage to provide enough mechanical strength for the cured material to fabricate samples with complex structures.

3. 3 Microstructure of printed samples

The Al_2O_3 green body components with complex shapes were obtained through optimized parameters. Sample images of the printed impeller of the Al_2O_3 green body are shown in Fig. 7. The printed green body had fine and complicated features, which could be well preserved without visible deformation after drying phase at 80 ℃. This was attributed to the homogeneous shrinkage of the material.

Figures 8(a) and 8(b) present SEM micrographs of the fractured surface of a printed Al_2O_3 green body sample. It could be seen that during the 3D printing process, the printed green body sample had no obvious defects or macroscopic pores (Fig. 8(a)). Besides, the grains were homogeneous and without apparent defects (Fig. 8(b)), indicating that the paste could be uniformly dispersed under high-speed mechanical agitation. Figures 8(c) and 8(d) present SEM micrographs of the fractured surfaces of the printed Al_2O_3 sintered samples.

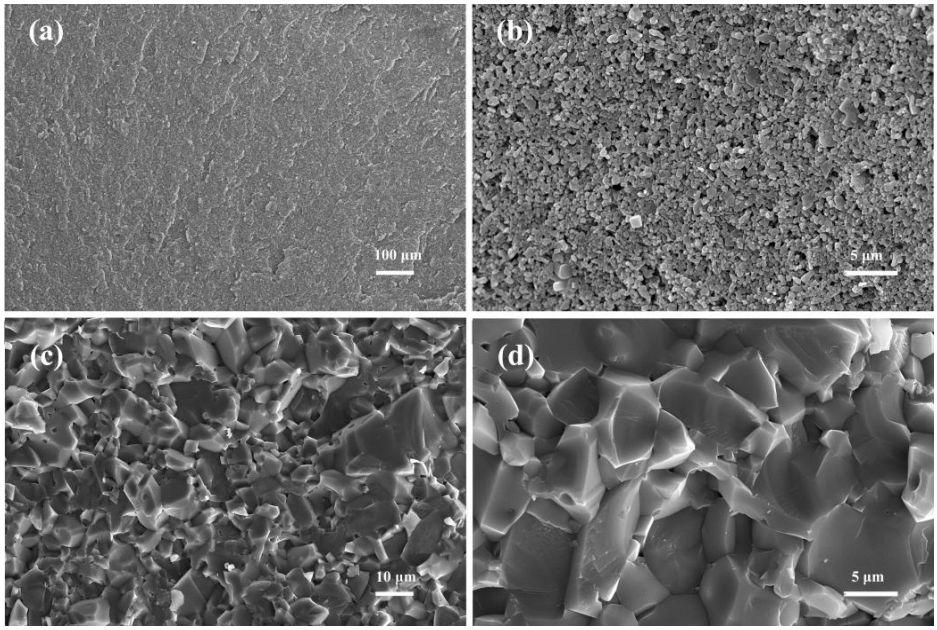

Fig. 8 SEM micrographs of the fractured surfaces of the printed Al_2O_3 samples: (a, b) the green body and (c, d) the sintered samples.

The sintered samples had a uniform microstructure with a relative density of 97.6%, a Vickers hardness of 18.91 Gpa, and a flexural strength of 250.86 MPa, respectively. These properties were not only attributed to the fine needles which could avoid the appearance of large pores at high solid loading, but also to the precise control of printing parameters. Therefore, adjusting the expansion in the pre-sintered material and using optimized thermally-induced process could preliminary fabricate the near net and intricate-shaped ceramic components with large inclined.

Further research studies will focus on the shrinkage of sintered ceramics with complex shapes and reducing the surface roughness of ceramics.

4 Conclusions

3D printing technology through DIW using thermally-induced solidifification was developed. The temperature of the slurry with carrageenan by thermally-induced was optimized, and the carrageenan content in the pastes was optimized. The paste consisting of 0.4 wt% carrageenan and thermally-induced about 55 ℃ could be rapidly solidified on the 3D printing. Inclined-plane alumina ceramic parts more than 60° were successfully prepared. Furthermore, the green body and sintered samples prepared by this 3D printing technology exhibited good homogeneity. The as-fabricated intricate-shaped engine blade samples with complex shapes would not collapse and exhibited a nearly pore-free structure, resulting in better uniformity of the green body.

Acknowledgements

The authors gratefully acknowledge the financial support from the National Key R&D Program of China (Grant No. 2017YFB0310400).

References

[1] Lewis J. Direct ink writing of 3D functional materials. *Adv Funct Mater* 2006, **16**: 2193–2204.

[2] Qin Z, Compton BG, Lewis JA, *et al*. Structural optimization of 3D-printed synthetic spider webs for high strength. *Nat Commun* 2015, **6**: 7038.

[3] Witek L, Shi Y, Smay J. Controlling calcium and phosphate ion release of 3D printed bioactive ceramic scaffolds: An *in vitro* study. *J Adv Ceram* 2017, **6**: 157–164.

[4] Kolesky DB, Truby RL, Gladman AS, *et al*. 3D bioprinting of vascularized, heterogeneous cell-laden tissue constructs. *Adv Mater* 2014, **26**: 3124–3130.

[5] McCracken JM, Badea A, Kandel ME, *et al*. Programming mechanical and physicochemical properties of 3D hydrogel cellular microcultures via direct ink writing. *Adv Healthcare Mater* 2016, **5**: 1025–1039.

[6] Sydney Gladman A, Matsumoto EA, Nuzzo RG, *et al*. Biomimetic 4D printing. *Nat Mater* 2016, **15**: 413–418.

[7] Siqueira G, Kokkinis D, Libanori R, *et al*. Cellulose nanocrystal inks for 3D printing of textured cellular architectures. *Adv Funct Mater* 2017, **27**: 1604619.

[8] Fu M, Chaudhary K, Lange JG, *et al*. Anisotropic colloidal templating of 3D ceramic, semiconducting, metallic, and polymeric architectures. *Adv Mater* 2014, **26**: 1740–1745.

[9] Zhou NJ, Liu CY, Lewis JA, *et al*. Gigahertz electromagnetic structures via direct ink writing for radio-frequency oscillator and transmitter applications. *Adv Mater* 2017, **29**: 1605198.

[10] Muth JT, Vogt DM, Truby RL, *et al*. Embedded 3D printing of strain sensors within highly stretchable elastomers. *Adv Mater* 2014, **26**: 6307–6312.

[11] Sochol RD, Sweet E, Glick CC, *et al*. 3D printed microfluidics and microelectronics. *Microelectron Eng* 2018, **189**: 52–68.

[12] Chen ZW, Li JJ, Liu CB, *et al*. Preparation of high solid loading and low viscosity ceramic slurries for photopolymerization-based 3D printing. *Ceram Int* 2019, **45**: 11549–11557.

[13] DeVries M, Subhash G, McGhee A, *et al*. Quasi-static and dynamic response of 3D-printed alumina. *J Eur Ceram Soc* 2018, **38**: 3305–3316.

[14] Chen ZW, Li ZY, Li JJ, *et al*. 3D printing of ceramics: A review. *J Eur Ceram Soc* 2019, **39**: 661–687.

[15] Liu Z, Song K, Gao B, *et al*. Microstructure and mechanical properties of Al_2O_3/ZrO_2 directionally solidified eutectic ceramic prepared by laser 3D printing. *J Mater Sci Technol* 2016, **32**: 320–325.

[16] Stumpf M, Travitzky N, Greil P, *et al*. Sol-gel infiltration of complex cellular indirect 3D printed alumina. *J Eur Ceram Soc* 2018, **38**: 3603–3609.

[17] Zengrong HU, Feng CHEN, Jiale XU, *et al*. 3D printing graphene-aluminum nanocomposites. *J Alloys Compd* 2018, **746**: 269–276.

[18] He RJ, Ding GJ, Zhang KQ, *et al*. Fabrication of SiC ceramic architectures using stereolithography combined with precursor infiltration and pyrolysis. *Ceram Int* 2019, **45**: 14006–14014.

[19] Zeng QF, Yang CH, Tang DY, *et al*. Additive manufacturing alumina components with lattice structures by digital light processing technique. *J Mater Sci Technol* 2019, **35**: 2751–2755.

[20] Shao HP, Zhao DC, Lin T, *et al*. 3D gel-printing of zirconia ceramic parts. *Ceram Int* 2017, **43**: 13938–13942.

[21] Ren XY, Shao HP, Lin T, *et al*. 3D gel-printing—An additive manufacturing method for producing complex shape parts. *Mater Des* 2016, **101**: 80–87.
[22] Shi YL, Wang WQ. 3D inkjet printing of the zirconia ceramic implanted teeth. *Mater Lett* 2020, **261**: 127131.
[23] Li N, Huang S, Zhang GD, *et al*. Progress in additive manufacturing on new materials: A review. *J Mater Sci Technol* 2019, **35**: 242–269.
[24] Rueschhoff L, Costakis W, Michie M, *et al*. Additive manufacturing of dense ceramic parts via direct ink writing of aqueous alumina suspensions. *Int J Appl Ceram Technol* 2016, **13**: 821–830.
[25] Deng LN, Feng B, Zhang Y. An optimization method for multi-objective and multi-factor designing of a ceramic slurry: Combining orthogonal experimental design with artificial neural networks. *Ceram Int* 2018, **44**: 15918–15923.
[26] Yang LL, Zeng XJ, Zhang Y. 3D printing of alumina ceramic parts by heat-induced solidification with carrageenan. *Mater Lett* 2019, **255**: 126564.
[27] Krishnamoorthy P. Sedimentation model and analysis for differential settling of two-particle-size suspensions in the Stokes region. *Int J Sediment Res* 2010, **25**: 119–133.
[28] Pritchard PJ. *Fox and McDonald's Introduction to Fluid Mechanics*, 8th edn. Manhattan, USA: John Wiley Inc., 2011: 38–40.
[29] Gregorová E, Pabst W, Štětina J. Viscoelastic behavior of ceramic suspensions with carrageenan. *J Eur Ceram Soc* 2006, **26**: 1185–1194.
[30] Ji MH. *Algae Chemistry*. Beijing, China: Science Press, 1997: 175–179. (in Chinese)
[31] Sason G, Nussinovitch A. Characterization of κ-carrageenan gels immersed in ethanol solutions. *Food Hydrocoll* 2018, **79**: 136–144.
[32] Tanusorn N, Thummarungsan N, Sangwan W, *et al*. Influence of carrageenan molecular structures on electromechanical behaviours of poly(3-hexylthiophene)/carrageenan conductive hydrogels. *Int J Biol Macromol* 2018, **118**: 2098–2107.
[33] Ortiz-Tafoya MC, Rolland-Sabaté A, Garnier C, *et al*. Thermal, conformational and rheological properties of κ-carrageenan sodium stearoyl lactylate gels and solutions. *Carbohydr Polym* 2018, **193**: 289–297.